

The Prefetch Aggressiveness Tradeoff in 360° Video Streaming*

Mathias Almquist
Linköping University, Sweden

Viktor Almquist
Linköping University, Sweden

Vengatanathan
Krishnamoorthi
Linköping University, Sweden

Niklas Carlsson
Linköping University, Sweden

Derek Eager
University of Saskatchewan, Canada

ABSTRACT

With 360° video, only a limited fraction of the full view is displayed at each point in time. This has prompted the design of streaming delivery techniques that allow alternative playback qualities to be delivered for each candidate viewing direction. However, while prefetching based on the user's expected viewing direction is best done close to playback deadlines, large buffers are needed to protect against shortfalls in future available bandwidth. This results in conflicting goals and an important prefetch aggressiveness tradeoff problem regarding how far ahead in time from the current playpoint prefetching should be done. This paper presents the first characterization of this tradeoff. The main contributions include an empirical characterization of head movement behavior based on data from viewing sessions of four different categories of 360° video, an optimization-based comparison of the prefetch aggressiveness tradeoffs seen for these video categories, and a data-driven discussion of further optimizations, which include a novel system design that allows both tradeoff objectives to be targeted simultaneously. By qualitatively and quantitatively analyzing the above tradeoffs, we provide insights into how to best design tomorrow's delivery systems for 360° videos, allowing content providers to reduce bandwidth costs and improve users' playback experiences.

CCS CONCEPTS

• Information systems → Multimedia streaming; • Networks → Application layer protocols;

KEYWORDS

360° streaming, optimized prefetching, view prediction

1 INTRODUCTION

Interactive video streaming is becoming increasingly popular, with 360° video leading the way. For example, since 2015 both YouTube (Mar. '15) and Facebook (Sep. '15) offer a rapidly growing selection of 360° videos that can be viewed in the browser on PCs, on smartphones, on tablets, or with head mounted displays (HMDs). 360° videos are typically recorded using an omnidirectional camera that captures every direction or by a collection of cameras whose video streams are stitched together into a single video [19]. When viewing these videos, users can freely choose to look in any viewing direction (e.g., by moving their head while wearing an HMD).

The flexibility in the users' choice of view (or region of interest) provides users an enriched viewing experience as they can explore a scene similar to as if they were at the location of the filming. However, this flexibility comes at the cost of significant bandwidth consumption when delivering these services over the internet.

360° videos are typically significantly larger than regular videos and can therefore consume a lot of bandwidth. However, similar to in everyday life, users have a limited field of view, resulting in only a small fraction (e.g., 20-30%) of the video data being needed for the actual viewing. Recently, this observation has prompted research into delivery techniques that allow alternative playback qualities to be delivered for each candidate viewing direction [4, 7, 16].

Clearly, delivery solutions that ignore the users' current field of view are likely to waste a lot of bandwidth delivering data that corresponds to scene data outside of this field of view or delivering higher than necessary data quality for scenes at the periphery of the field of view. In the ideal case, a content provider would be able to perfectly predict both the head movements and future bandwidths so that it could deliver only the data that the user views, at the highest possible quality allowed by the time-varying available bandwidth. Unfortunately, neither head-movement prediction nor bandwidth prediction is perfect. Content providers wanting to deliver these services effectively over the internet therefore face the following two challenges.

First, content providers must take into account the uncertainty in the user viewing directions and the impact that changes in viewing direction may have on the perceived playback quality. Second, as with regular streaming, video data must be buffered at the clients so to protect against playback stalls caused by (future) bandwidth variations. Maintaining a reasonably large playback buffer is particularly important when using HTTP-based Adaptive Streaming (HAS) solutions such as those used by the most popular international streaming services (e.g., YouTube, Facebook, Apple, Netflix) and most regional streaming providers, and that are currently being standardized through MPEG-DASH. Such services typically download 2-5 second chunks using HTTP(S) and try to maintain significant buffers (e.g., 10-120 seconds, depending on service and type of network device) to account for today's networks being best-effort with significant bandwidth variations being common.

While much work has been done to study quality adaptation algorithms for regular non-360° videos [27], for which the user viewing direction is fixed, to the best of our knowledge, no prior work has considered the problem of prefetching aggressiveness (i.e., how far ahead in time from the current play point should prefetching be done), for 360° videos where the user viewing direction may vary. In this work we present the first such study. This is an important problem for wide-area delivery techniques, since here the

*This paper is an extended version of our original *ACM MMSys* 2018 paper [3]. It is posted here by permission of ACM for your personal use, not for redistribution. Please cite our original paper (with the same title) published in *ACM Multimedia Systems (MMSys)* '18, Amsterdam, Netherlands, June 2018. <https://dx.doi.org/10.1145/3204949.3204970>

need to protect against shortfalls in future available bandwidth and the need to quickly respond to changes in user viewing direction result in conflicting goals. To see this, note that the need to protect against future bandwidth drops motivates building up a large buffer (i.e., aggressively prefetching well-ahead of the current play point). On the other hand, prefetched data can be worthwhile only if the data will be within the user’s field of view. Use of a small prefetch buffer is motivated by the observation that prediction of the user viewing direction is most accurate over short time scales.

Figure 1 illustrates the dependency between uncertainty in the user viewing direction, and the time scale, using four categories of videos (each category defined in Section 3). For all categories, we show the relative probability distributions of the change in the viewing direction of a set of example users viewing the same subset of videos, conditioned on the time duration T (in seconds), where $T=2s$ (left) and $T=20s$ (right). The origin in the figure corresponds to no change and all changes are measured relative to the viewing direction the user had T seconds earlier. It is clear from these results that the playback quality selection for each potential viewing direction can be best optimized when done very close to the playback of a frame, suggesting the use of small buffer margins. This shows that there is an important tradeoff between the goal of making good prefetching decisions with respect to the quality that should be prefetched for each direction, and the goal of prefetching far ahead in time, so to protect against future bandwidth variations or other randomness causing stalls.

This paper presents a measurement-driven characterization of the prefetching aggressiveness tradeoffs associated with different categories of 360° videos, providing both qualitative and quantitative insights regarding how best to address these tradeoffs. In particular, we present a characterization of the user behavior, as well as an optimization framework that captures the prefetching aggressiveness tradeoffs experienced by a content provider wanting to optimize the quality selection in each viewing direction so to maximize the user’s expected quality of experience (QoE). The optimization framework takes into account both the probability of the user having a particular viewing direction at a particular point in time, and the buffer levels needed to avoid playback interruptions.

Our optimization framework assumes the use of chunk-based streaming (e.g., using DASH or alternative HAS-based formats) and takes into account the viewing behaviors we observe for different categories of 360° videos. Using measurements from our user study and our optimization framework, we provide insights into the best possible tradeoffs when delivering 360° videos over the internet. Our main contributions are as follows:

1) *User-driven head-movement characterization:* We record the orientation and rotation velocity of an Oculus Rift HMD during playback of different categories of 360° videos. More than 21 hours of viewing data (based on the viewing of 32 participants) is analyzed to characterize viewing patterns relevant for optimizing the wide-area delivery of 360° video. Significant differences in the viewing patterns between the different categories are observed. However, for most video categories the head movements (e.g., as in Figure 1) are sufficiently confined that, although viewing direction prediction is most accurate at short time scales, prefetching with optimized quality selection can also be beneficial at larger time scales.

2) *Optimized buffer-quality tradeoffs:* We present an optimization framework that captures the optimal tradeoffs between the goal of prefetching far ahead in time (to protect against bandwidth variations and stalls) and the goal of making the best quality selections for each potential viewing direction when prefetching so as to maximize the expected playback utility (as is dependent on the probability distribution of the user’s viewing direction when a particular play time is reached, and the qualities of the prefetched chunks for this play time). Using this framework we then evaluate the optimized tradeoffs for different categories of videos, utility functions, and bandwidth conditions. Our evaluation highlights differences across video categories and the possible impact of how bandwidth constrained clients are.

3) *Discussion of further design optimizations:* Finally, based on our findings, we present an adaptive policy framework and describe additional optimizations that could be done to improve client performance for the different video categories. The framework allows clients to simultaneously protect against bandwidth variations and provide personalized and content-based quality adaptation, best optimized at shorter time scales. Using our measurements, we then discuss additional optimizations that leverage biases in head movements related to the current rate of change in the viewing direction, the relative viewing direction compared to that at the start of the video, and if the viewer is in an initial exploration phase (that we have observed) or not.

The remainder of the paper is organized as follows. Section 2 provides a brief introduction to 360° video. Our measurement methodology and dataset are described in Section 3. Section 4 presents a characterization of the observed head movements, before Section 5 presents our optimization framework and characterizes the prefetch aggressiveness tradeoffs. Motivated by these tradeoffs and observations, Section 6 then presents an adaptive framework that allows both substantial prefetching well ahead of playback deadlines and fine grained quality adaptation based on predicted viewing directions, followed by a data-driven characterization of some further considerations that such a system could account for. Finally, Section 7 presents related work and Section 8 concludes the paper.

2 BACKGROUND

360° videos provide users with an interactive video experience, in which the users can freely select any viewing direction within a spherical virtual environment. Users can experience 360° videos in several ways. On a PC, the user typically controls the view using either the W-A-S-D keyboard buttons or by clicking and dragging using the mouse. On a smartphone or tablet, the user can change the view by swiping the screen or by changing the orientation of the phone/tablet. Finally, with virtual reality (VR) head mounted displays (HMDs), the users simply move their heads in the same way as if they were at the location where the video was recorded, creating a more immersive experience.

In this project, we use the first consumer version (CV1) of the Oculus Rift headset, released March 2016. The Oculus Rift hardware system consists of a sensor, a headset, and a remote. The headset works as a display using OLED panels with a resolution of 1080x1200 per eye, resulting in 2160x1200 across the entire field of

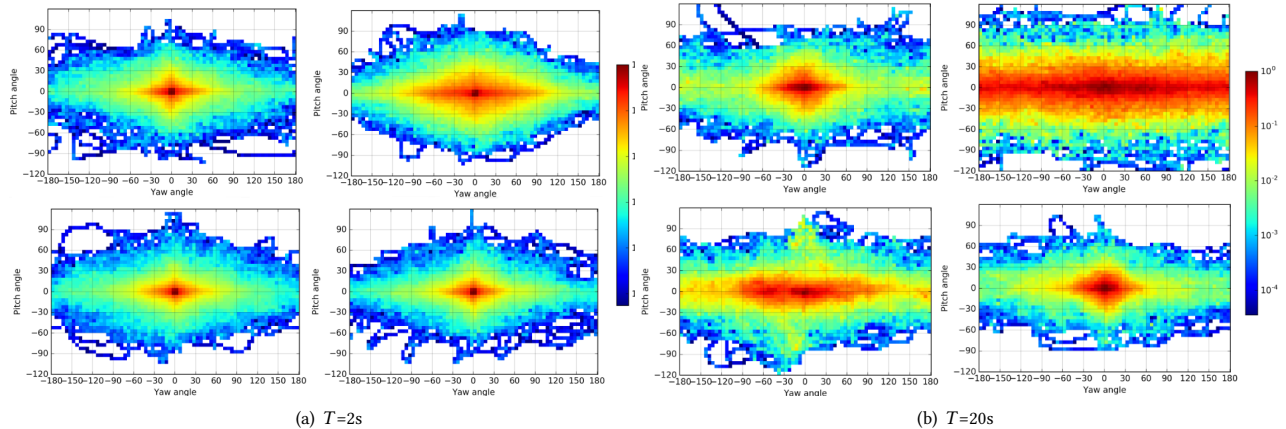


Figure 1: Example heat-maps for four categories of videos. Within each subfigure: Rides (top-left), Exploration (top-right), Moving focus (bottom-left), Static focus (bottom-right).

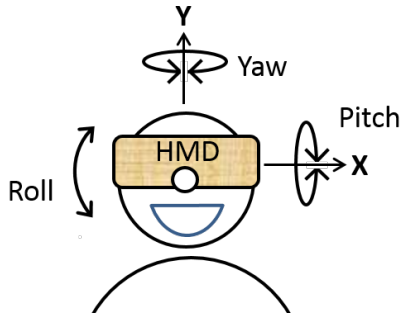


Figure 2: Head-movement coordinates: Yaw, pitch, and roll.

view. Oculus offers a 110° horizontal field of view. The VR applications run on a PC which transfers video and audio to the headset via an HDMI cable. To allow users to move in the virtual space, the sensor offers position tracking by monitoring infrared LEDs that are embedded in the headset. The remote can be used for navigation, but was not needed for our experiments.

The headset features a set of Micro-Electro-Mechanical System (MEMS) sensors, namely a magnetometer, gyroscope and an accelerometer which are combined so as to track the orientation of the headset [15]. The headset orientation is interpreted according to an internal virtual coordinate system, transmitted from the headset to the PC at a rate of 1000 Hz. This allows applications to accurately track a user’s head movements and update the view accordingly.

3 MEASUREMENT METHODOLOGY

We next describe our measurement setup.

Physical setup: We used a dedicated PC with Intel Xeon CPU E5-1620 V4 3.50GHz, 32GB RAM, and a NVIDIA GeForce GTX 1080 graphics card. The PC ran Windows 10 and was connected to the Oculus Rift CV1 headset and sensor via USB 3.0. To deliver audio and visuals, an HDMI cable was connected directly between the headset and the HDMI port of the dedicated graphic card of the PC. Once connected, the sensor was placed on a table facing towards an open area in the room where the user wearing the headset was placed on a turning chair approximately 1.5 meters away.

Sensor readings and viewing traces: Sensor readings were extracted using the Oculus Software Developer Kit (SDK) 1.8.0 and Oculus runtime 1.9.0 291603. For this purpose, we developed a minimal application in C++ that extracts the head orientation and rotation velocity from the MEMS sensors. For easy interpretation, we convert orientation readings (from quaternions) to yaw-pitch-roll format based on the user’s head orientation relative to that at the start of each video and velocities to degrees per second. The yaw-pitch-roll format is illustrated in Figure 2. Here, all directions are measured relative to the 0° line. Importantly, to allow direct comparison of the viewing directions within a scene, for yaw ($\pm 180^\circ$), we set the 0° line on a per-video basis. In particular, rather than using the direction of the sensor (default) as zero line, we instead use the head orientation that the user has at the start of the video. The reason for this is that videos are played relative to this initial viewing direction. This adjustment ensures that we record the same yaw angle for two users looking at the same object at the same time instance within a video, regardless of their original head positioning. For pitch ($\pm 90^\circ$), the 0° line is parallel to the ground, and for roll the zero value corresponds to holding the head straight.

Video playback and recording: Our application utilizes the Whirligig video player¹ to sequentially play a list of mp4 videos stored locally on the PC. For each video viewing, the user’s head orientation and movements are recorded and stored to trace files.

Video selection: We first identified 30 videos from YouTube’s 360° collection that we found nicely represented different categories of 360° videos. We then used the trace collector application to download these videos in 4K resolution, ensuring that we can offer good quality of experience during viewing. The videos are 1-5 minutes long (3 min on average) and divided into five categories.

- *Exploration:* In these videos, there is no particular object or direction of special interest and the users are expected to explore the entire sphere throughout the video duration. Furthermore, two independent viewers of the same video are expected to have substantially different viewing angles at each point in time. (Example: Camera positioned on top of a tall building overlooking a city.)

¹<https://www.oculus.com/experiences/rift/1130182873666293/>

- *Static focus*: In these videos, the main focus of attention is deemed to always be at the same location in the video. A static viewing behavior is expected since the focus of attention does not move. With these videos, most of the time a near-zero yaw angle is expected. (Example: A theatre performance or a concert being displayed on a scene.)
- *Moving focus*: Story-driven videos where there is an object of special interest that is moving across the 360° sphere. With these videos, a high correlation is expected between the viewing angles of users over time, since they typically would follow the objects of interest. (Example: An action scene where the involved characters move around the viewing sphere, causing the user to follow.)
- *Rides*: In these videos, the users take a virtual ride in which the camera is moving forward at a high speed, making users feel that they too are moving forward quickly. In the majority of the video the user is expected to look forward, as when taking a ride in real life. (Example: Roller-coaster.)
- *Miscellaneous*: This category includes videos that were deemed to have a mix of the characteristics of the other categories or had a hard-to-classify “unique feel” to them.

The full set of videos and their categorization are summarized in Table 1. We note that some of these categories are named in part based on the expected viewing behavior of a user watching the video. We believe that this allows for a natural categorization that can be used on larger sets of videos. Of course alternative classifications are possible. However, for the purpose of this study, this categorization is sufficient to characterize and evaluate how the differences in viewing behavior of these diverse categories impact the best prefetching tradeoffs.

User study: An open invitation was sent out to different groups at the university, allowing people to sign up for one-to-three 45-minute sessions (but at most one per day). In total, 32 people signed up for a total of 45 sessions. To avoid bias in the results and encourage viewers to follow their instincts, at the start of each session, users were not given any instructions on how to view a video, but instead simply watched a four minute introduction video about VR produced by Oculus. This allows the user to get accustomed to the 360° surrounding and feel comfortable wearing the headset. After the introduction, the participants then view ten “semi-random” videos. Videos for each session are selected at random from the set of videos that the user has not viewed in the past (so that users attending multiple sessions do not watch the same video twice) and we make sure that all users watch one “representative” video from each category (first video in each row of Table 1).² After the views to the representative videos had been accounted for, the other videos got between 8-13 views each. The additional views to the “representative” videos allows for more detailed analysis for these videos. It should also be noted that some videos were avoided for users that indicated that they had fear of heights or were prone to motion sickness or dizziness (asked at the start of the session). Finally, to avoid biases related to the order videos are played, the order of the videos selected for a given session is randomized.

²By definition, it is impossible to choose a “representative” video for the Miscellaneous category. However, due to sports-related follow-up work, we selected a video (“Hockey”) in which viewers watch a hockey game from between the player benches.

In total, we recorded the head movements from 439 unique viewings, totaling 21 hours and 40 minutes. The age distribution of the 32 participants was: 20-29 (66%), 30-39 (28%), 40-49 (3%), 50-59 (3%). 56% of the participants were male and 44% female. Moreover, 25 participants had never tried VR and only 3 had tried it with Oculus.

No personal information is stored or included in our datasets. For our analysis we only perform per-category and per-video analysis, no per-user analysis, and only aggregate information is reported. We present results for the four more well-defined categories *rides*, *exploration*, *moving focus*, and *static focus* (excluding the *miscellaneous* category). Finally, we note that we did not make any modifications to the videos or otherwise try to effect the user experience. The users simply watched the videos as they otherwise would, while we used the API to record their head movements.

4 CATEGORY-BASED CHARACTERIZATION

4.1 Angular utilizations

We begin by looking at how the viewing angles have been utilized for the videos of the different categories. Figure 3 shows a heatmap of the most utilized yaw and pitch angles over the full duration of the videos. A quantification of the angular utilizations (also including the roll) is provided in Figure 4. Here, for each category, we show the cumulative distribution function (CDF) of the observed angles for yaw (red), pitch (green) and roll (blue).

We note that yaw is the most dominant orientation movement across all categories, with angular utilizations much more widely distributed than for pitch and (especially) roll. This suggests that predicting and accounting for changes in yaw, is most important when trying to adapt the prefetch quality based on the expected viewing direction by the time a prefetched frame is played.

In general, for the videos that we selected, the distributions are relatively symmetric. Except for the moving focus category (bottom-left), for which there is a slight bias towards the left, we do not see any major biases between leftwards or rightwards utilizations. The slight bias observed for the moving focus videos is likely due to the particular choice of videos. Furthermore, except for the exploration videos, there is only a very small bias to look downwards rather than upwards. For the exploration videos this bias is reinforced by videos (taken in Dubai) where the viewer is positioned at the top of a very large building or when flying above the city. For roll, we observe only small non-biased changes over the video playback durations (e.g., 98% within $\pm 10^\circ$).

Finally, and perhaps most importantly, both Figures 3 and 4 clearly show that there are significant differences in the angular utilizations between the different categories. For example, if we focus on the (dominant) yaw-angle distributions, we observe substantially more evenly spread angular utilization with the exploration (top-right) videos than with the rides (top-left) and static focus (bottom-right) videos. With both these latter categories, users spend most of the time in the original direction (e.g., 80% of the time within $\pm 30^\circ$ and 90% within $\pm 60^\circ$) in which the video playback was initiated. These results show that for these categories of videos, the original (or intended primary) viewing direction can be used as a good predictor of what directions to prioritize aggressively prefetching data for future playback.

Table 1: Summary of videos. (To watch video, use URL of the form: <https://www.youtube.com/watch?v=VideoID>, where VideoID is replaced based on the table entries.

Category	Video Name (Duration, VideoID)
Exploration	Zayed Road (3:00, uZGrikvGen4), Burj Khalifa (2:30, bdq4H1ClehI), Hadrain's Wall (3:36, 2zeKpeRZ8uA), New York (1:59, T3e-GqZ37uc), White House (5:16, 98U2jdk8OGI), Waldo (1:00, hM9Tg_dQkxY), Skyhub (4:00, D9-i_F3xYhI)
Static	Christmas Scene (2:49, 4qLi-MnkxBY), Boxing (3:29, raKh0OIERew), Elephants (2:49, 2bpICIClAIg), Mongolia (1:52, VuOfQzt2rI0), Orange (2:43, i29ITMfLVU0)
Moving	Christmas Story (4:14, XiDRZfeL_hc), Assassin's Creed (2:31, a69EoLiYqoE), Clash of Clans (1:23, wczdECcwRw0), Frog (3:13, sk8hm7DXD5w), Solar System (4:32, ZnOTprOTHc8), Invasion (4:04, gPUDZPWhiiE)
Rides	F1 (1:54, 2M0inetghnk), Le Mans (3:00, LD4XfM2TZ2k), Roller Coaster (2:11, LhfkK6nQSow), Total War (1:49, YSBWwnOHvM8), Blue Angels (2:30, H6SsB3YqQg), Ski (2:48, kMCYo5rO6RY)
Misc.	Hockey (2:25, 8DKVvb17xsM), Tennis (4:05, U-_yX4e4Z_w), Avenger (2:58, 3LSf6_ROCdY), Trike Bike (3:14, jU-pZSsYhDk), Temple (4:36, Lx14NDttRWo), Cats (1:59, 0RtmVnD8_XM)

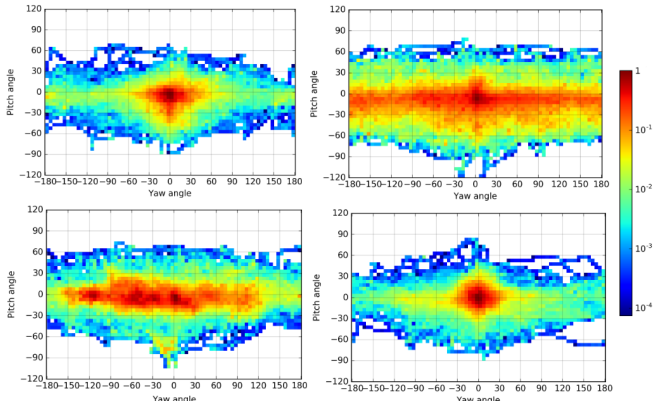


Figure 3: Heatmap of most utilized yaw and pitch angles: Rides (top-left), Exploration (top-right), Moving focus (bottom-left), Static focus (bottom-right).

While the angular utilizations (Figure 4) of the moving focus (bottom-left) videos are more similar to those of the exploration videos (top-right), we have found that these videos differ substantially in how predictable the movements are. This is illustrated in Figure 5. Here, we show the average angle difference between each pair of users watching the same video, as a function of the playtime (with time-axis constrained by the duration of the shortest video).

In contrast to the results shown in Figure 4, Figure 5 shows that the average angle difference between each pair of users watching the same moving focus (bottom-left) video is more similar to that for rides (top-left) and static focus (bottom-right) videos than for exploration (top-right) videos. These results suggest that the viewing patterns of other users who have watched moving focus, rides, and static focus videos are valuable when predicting the viewing directions of future viewers; hence, allowing better prefetching when differentiating the quality for different directions.

Figure 6 provides a more concrete example of how different viewers may have similar viewing patterns despite using the full spectrum of yaw angles. Here, we show the yaw angle for four example viewers as they watch the same moving focus video (in which the viewer is taken on a narrated journey through the solar system). The above results suggest that we use a reasonable categorization of videos, in which each category has distinct properties visible in the observed viewing characteristics. Note in particular, from Figure 5,

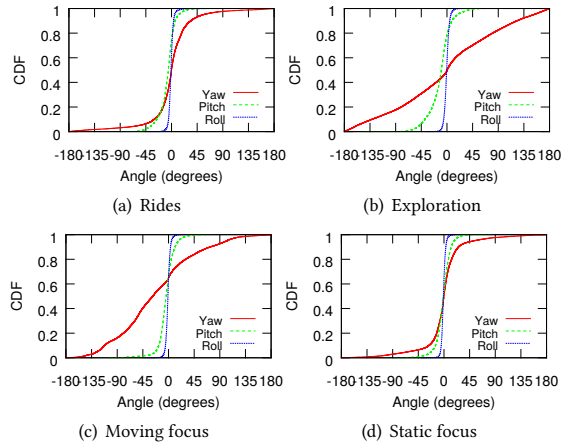


Figure 4: CDFs of angle utilization.

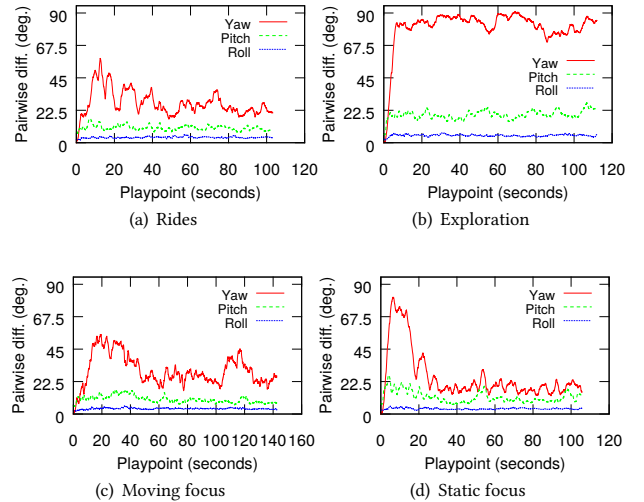


Figure 5: Average pairwise angular difference between users.

the considerably different behavior for the exploration (top-right) videos. For this category of videos, the average pairwise difference is only slightly within 90° (where 90° corresponds to the average

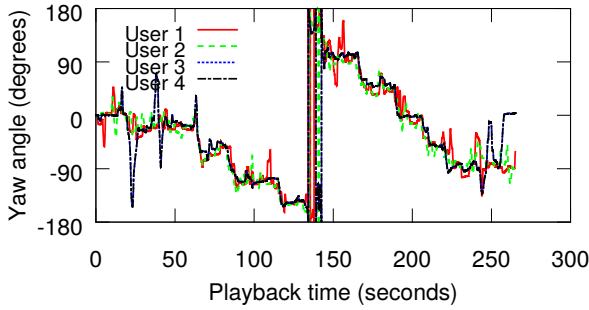


Figure 6: The yaw angle over time for four example users watching the “Solar system” video.

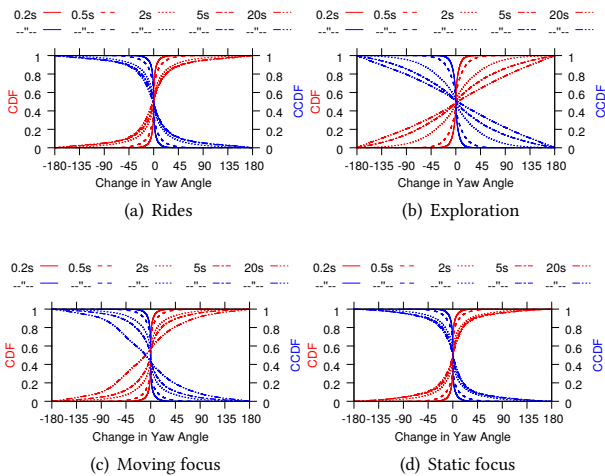


Figure 7: CDFs and CCDFs of the yaw change over different time intervals T .

pairwise difference that would be observed if viewing directions were random). Clearly, users watching these videos tend to move completely independently, focus on highly different things, and have mostly uncorrelated viewing angles for the full video duration.

Finally, we note that there often appears to be some exploratory behavior when viewing the videos of the other categories as well, in particular at the beginning of a video. This is particularly visible when considering the static focus (bottom-right) videos in Figure 5. Here, we see a substantial initial spike in the pairwise angular differences between users during the first 20 seconds of the playback. This suggests that users tend to explore once they are put in a new environment, as at the start of a new video. We will examine this further in Section 6.

4.2 Changes in Viewpoint

For shorter time scales, one of the most natural and commonly used predictors of a user’s future viewpoint is the current viewpoint. However, since users can quickly turn their head or body, when using such a predictor, it is important to understand how such viewpoint changes vary across different categories of videos and how the absolute changes depend on the time T over which the

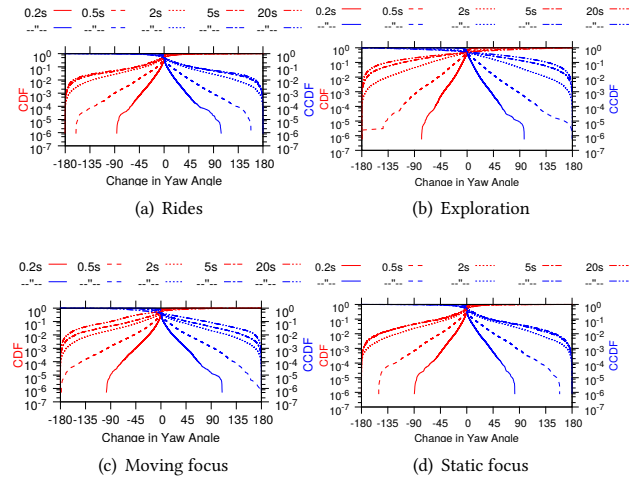


Figure 8: Log-scale version of Figure 7.

change is measured. We next take a closer look at how much the viewpoint differs between two time points separated by T seconds.

To cover a wide range of 360° delivery technologies we consider time intervals T between 0.2 seconds to 20 seconds. Here, the low-end intervals (e.g., 0.2-1 second) may be most applicable for low-latency scenarios where edge servers are used to render frames that the users may view and the multi-second range (e.g., 2-20 seconds) may be most applicable for HAS-based designs, which typically use 2-10 second chunks and typically must account for significant wide-area bandwidth variations.

In both scenarios, we foresee either the client adapting the qualities it requests for each direction based on view change probabilities or the servers adapting the qualities for each direction based on the user’s current viewing direction and statistics about view change probabilities. Note that some buffering is necessary in all scenarios as the human tolerance threshold for differences in the displayed content and the actual viewing direction is approximately 50 ms [1, 2, 5] and at the minimum we must account for network jitter and other network effects, which may be on the order of 100 ms or more in modern LTE networks, for example [29]. Further delays beyond 50 ms can result in user discomfort and motion sickness.

Figure 7 shows the CDFs and Complementary CDFs (CCDFs) of the change in the yaw angle for each of four video categories. For the short time scales (e.g., 200ms) we have only observed very minor differences between the video categories. The extreme values (i.e., the tail values) of these distributions are bounded by the speed with which the participants moved their heads when watching the videos. For example, for all categories 99% of the head movements are within $\pm 28^\circ$ yaw angle and $\pm 13^\circ$ pitch angle. The corresponding numbers for 99.9% are: $\pm 46^\circ$ and $\pm 19^\circ$, respectively. Across all experiments, the largest changes that we observe over 200ms are 95° for yaw and 35° for pitch. Again, the maximum is almost the same for all four video categories.

The above 200 ms results suggest that a significant portion of the potential viewing field may not need to be pre-rendered in edge-based rendering systems operating at the extremely low-latency (i.e., sub-200 ms) time scale. However, modern networks do not

provide performance guarantees sufficient to operate at such time scales yet [29]. Instead, most video streaming services today therefore require substantial buffers to protect against bandwidth variations and other interruptions, and HAS-based solutions with larger buffers are likely to continue to dominate the markets for the foreseeable future.

Considering head movements over longer time scales, for all categories the full range (i.e., $\pm 180^\circ$) of head movements is covered already after a second. In fact, for the explore and moving focus categories, we observe such full range yaw rotations already at the 0.5 second time scale. For the rides and static focus videos the most extreme movements reach at most 100° and 90° , respectively, over this 0.5 second time window. To better quantify these extreme changes in viewing direction, Figure 8 presents log-scale versions of the Figure 7 plots.

Overall, we observe diminishing increases in the variations as the time interval T increases and the distributions become more similar to the life-time distributions (shown in Figure 4). This is most clear for rides and static focus. For these categories, the differences between the 5-second and 20-second curves are much smaller than for the other neighboring curves and the 20-second curves provide similar accuracy as when using the life-time distribution, suggesting that for these two categories it is equally good to use the current viewing direction as the zero-degree line (used for the life-time distributions) as predictors when maintaining a 20-second buffer.

In general, as the buffer needed becomes greater, the more value should be placed on the angular distribution and the viewpoint directions of other users that have watched the same video, for example. This is particularly apparent when considering the moving focus category (e.g., as exemplified in Figure 6). For this category we also see that the current direction is a slightly better predictor than the zero-degree line. Interestingly, for the exploration category, on the other hand, the zero-degree line is a (slightly) better predictor for the 20-second time scale. To see this, note that the 20-second distribution for the exploration category closely resembles that of a uniform distribution (showing that yaw-based angular prioritization has no benefit for the exploration category when maintaining a 20+ second buffer), whereas the life-time distribution is somewhat more concentrated around the zero-degree line.

In summary, our results show clear differences in the viewpoint distributions and how predictable the head movements are (e.g., as measured by how concentrated distributions are), both across video categories and with regards to the time scale over which prediction is done. We next determine the (optimized) tradeoffs between the buffer used and the expected achievable playback utility.

5 OPTIMIZED PREFETCHING TRADEOFF

Let us now consider the basic prefetch aggressiveness tradeoff between clients trying to maintain a buffer T (to protect against stalls due to bandwidth variations or other service interruptions) and the expected playback utility $E[u|T]$ experienced by the client, where we use playback utility to measure the client's perceived playback quality. To better understand this tradeoff we consider the optimized prefetch schedule of a client that operates in steady-state, maintaining a fixed buffer of T seconds, and that prefetches data at a known average download rate D . For this client, we then

determine the optimized prefetch schedule for different buffer levels T , allowing us to investigate the tradeoff between the optimized $E[u|T]$ and T .

5.1 High-level optimization model

Without loss of generality, consider the optimized download schedule of an arbitrary chunk with playback duration Δ . For each viewing direction θ_n of such a chunk we assume that the player can choose a tile n of quality level l ($0 < l \leq L$) with encoding rate $q_{n,l}$ or to not download any data for that direction. We use $l = 0$ to indicate this last choice. Furthermore, we assume that each tile can be delivered independently (or together with other tiles, as a combined chunk) and that these tiles can be stitched together either at the client or at the server (when creating a combined chunk).

For simplicity, since the majority of the head movements are yaw rotations (with small pitch and negligible roll), we will focus our analysis here on the yaw angle. We also discretize the possible angles (possible viewing directions). In particular, we let directions $n = 0, 1, \dots, N - 1$ correspond to increasing yaw angles from the initial viewing direction, with wrap-around when $n = N$ (i.e., direction N is the same as the initial viewing direction, direction 0). Each of these viewing directions corresponds to a single tile. Note that the entire view field at any point in time may encompass a number of these tiles. Generalizations that also take into account pitch are relatively straightforward, whereas models that also take into account roll require significantly more geometry and notation.

At a high level, given the available bandwidth budget in the next Δ seconds, an average buffer of T , and a known conditional probability distribution $p_n(T)$ that the user looks in direction n another T seconds after the chunk was requested by the client, we maximize the expected playback utility:

$$E[u|T] = \sum_{n=0}^{N-1} p_n(T) u(n|q_0, q_1, \dots, q_{N-1}), \quad (1)$$

where $u(n|q_0, q_1, \dots, q_{N-1})$ is the playback utility experienced by the client when looking in direction n after having prefetched tile qualities q_0, q_1, \dots, q_{N-1} for the N directions. For the purpose of our numeric evaluation, we calculate the probabilities $p_n(T)$ as follows:

$$p_n(T) = \int_{\theta_n}^{\theta_{n+1}} p(\theta|T) d\theta, \quad (2)$$

where θ_n is the yaw angle corresponding to direction n , using CDFs such as those studied in Section 4.

To model the expected utility $u(n|q_0, q_1, \dots, q_{N-1})$, we use a utility model that weights (i) the playback utility $u(q_n)$ of the encoding rate q_n in the current viewing direction n , (ii) the playback utility of neighboring viewing directions (i.e., $u(q_{n-1})$, $u(q_{n+1})$), and (iii) the relative utility differences compared to neighboring directions (i.e., $-|u(q_n) - u(q_{n-1})|$ and $-|u(q_n) - u(q_{n+1})|$), the last of which potentially may cause negative effects. Since we are not aware of any research that has provided relative weights to these factors for the context of 360° videos, we use variable-sized weights and evaluate their relative importance. It turns out that by careful selection of constants, only a single parameter β is needed. To see this, let us give each of the above factors the relative weights (i) $(1 - \alpha - \beta)$, (ii) $\frac{\alpha}{2}$ times their probability ratios ($\frac{p_{n-1}}{p_n}$ and $\frac{p_{n+1}}{p_n}$),

and (iii) $\frac{\beta}{2}$, respectively. Summing over all directions, the objective function can now be simplified as follows:

$$\begin{aligned}
E[u|T] &= \sum_{n=0}^{N-1} p_n \left((1 - \alpha - \beta)u(q_n) + \frac{\alpha}{2} \left(\frac{p_{n-1}}{p_n} u(q_{n-1}) + \frac{p_{n+1}}{p_n} u(q_{n+1}) \right) \right. \\
&\quad \left. - \frac{\beta}{2} (|u(q_n) - u(q_{n-1})| + |u(q_n) - u(q_{n+1})|) \right) \\
&= (1 - \beta) \sum_{n=0}^{N-1} p_n u(q_n) - \beta \sum_{n=0}^{N-1} \frac{p_n + p_{n+1}}{2} |u(q_n) - u(q_{n+1})|. \tag{3}
\end{aligned}$$

Here, we have dropped the argument T from $p_n(T)$ and used q_n to represent the selected encoding rate for direction n . Note that this expression is independent of α .

Discussion of utility model: Similar HAS/DASH models have been used to capture the quality of experience (QoE) of “regular” non-interactive streaming video, rather than 360° video. For example, Yin et al. [33] try to capture the QoE by the following metrics: (i) the average video quality, (ii) the average quality variations, (iii) number and duration of rebufferings, and (iv) the startup delay. Looking at a single chunk during steady-state streaming, the startup delay and average quality variations are not applicable to our model. Instead, we use the expected buffer (T) to capture the protection against stalls/rebufferings (i.e., factor (iii)) and consider the quality variations relative to nearby viewing angles, in the case that a user changes viewing direction and also to take into account that the viewfield, especially the peripheral view, typically will be made up by tiles from neighboring directions. It is therefore good if the quality differences between neighboring tiles are not too obvious. We note that this objective will somewhat offset greedy maximization of the average (expected) video quality, and weight the two factors using a variable β ($0 \leq \beta \leq 1$).

5.2 Detailed optimization model

Let $q_{n,l}$ denote the video encoding rate of tile n with quality level l (ordered from lowest to highest quality), let $b_{n,l} = b(q_{n,l})$ denote the size of the tile (proportional to its encoding rate), let $u_{n,l} = u(q_{n,l})$ denote the estimated playback utility of this tile, and let $x_{n,l}$ be a binary decision variable (indicating that tile n of the chunk is downloaded at quality level l whenever $x_{n,l} = 1$). (See Table 2.) We can now formulate the problem of choosing optimal quality encodings as a packing problem:

$$\text{maximize } E[u|T], \tag{4}$$

where

$$\begin{aligned}
E[u|T] &= (1 - \beta) \left(\sum_{n=0}^{N-1} p_n(T) \sum_{l=0}^L x_{n,l} u_{n,l} \right) \\
&\quad - \beta \left(\sum_{n=0}^{N-1} \frac{p_n(T) + p_{n+1}(T)}{2} \right. \\
&\quad \left. \times \sum_{l=0}^L \sum_{l'=0}^L x_{n,l} x_{n+1,l'} |u_{n,l} - u_{n+1,l'}| \right), \tag{5}
\end{aligned}$$

Algorithm 1: Calculate optimal single-slot prefetch schedule.

Input: Number of directions N , total bytes to download ΔD , probabilities p_n , tile sizes $b_{n,l}$, and utilities $u(q_{n,l})$.

Output: Optimal set of qualities (equivalent to $x_{n,l}$) and value of the corresponding (optimal) objective function.

```

1 foreach  $0 \leq l_0 \leq L$  do
2   foreach  $0 \leq C \leq \Delta D$  do
3     foreach  $0 \leq n \leq N - 1$  do
4       foreach  $0 \leq l \leq L$  do
5          $DP(l_0, l, n, C) \leftarrow$  equation (9)
6 Return  $\max_{0 \leq l_0 \leq L} DP(l_0, l_0, N - 1, \Delta D)$  and corresp. parent pointers;
```

such that

$$\sum_{l=0}^L x_{n,l} = 1, \quad 0 \leq n < N, \tag{6}$$

$$\sum_{n=0}^{N-1} \sum_{l=0}^L x_{n,l} b_{n,l} \leq \Delta D, \tag{7}$$

$$x_{n,l} \in \{0, 1\}, \quad 0 \leq n < N, 0 \leq l \leq L. \tag{8}$$

As is typically the case, for our evaluation, we assume that $u(q_{n,l})$ is a concave function of $q_{n,l}$ and that $b_{n,l}$ is a linear function of $q_{n,l}$. Furthermore, we model the case when there is missing data (i.e., when $x_{n,0} = 1$) using $b_{n,0} = 0$ and a negative utility $u_{n,0} = -f u_{n,L}$, where f is a penalty factor.

For the special case that $\beta = 0$, the above problem simplifies to the standard 0-1 knapsack problem. It is therefore trivial to formulate any 0-1 knapsack problem using our formulation, and our problem is therefore at least as hard as the 0-1 knapsack problem, which is NP-complete. As with the standard 0-1 knapsack problem, under some circumstances this problem can be solved using dynamic programming. We next describe one such formulation and then discuss variations thereof.

5.3 Dynamic programming solution

For simplicity, in the following, we assume that the size $b_{n,l}$ of each tile, as well as the amount of data that can be downloaded during the interval Δ (i.e., ΔD), can be represented using integers (e.g., measured in kilobytes).³ Under these assumptions, given a list of tiles, we can formulate the sub-problem of determining the maximum utility for directions $0:n$, given a total prefetching capacity C for these directions. To allow us to take into account both the utility differences between neighboring tiles and operation over a circular space (with modulus N), we also condition each sub-problem on the encoding selections for tiles 0 and $n + 1$. Denoting the quality selections for tiles $n + 1$ and 0 by l and l_0 , respectively, we can write

³The development of $(1 + \epsilon)$ FPTAS approximations appear possible when these quantities are non-integers.

Table 2: Notation for streaming model for a single chunk.

Symbol	Definition
L	Number of non-zero quality levels of the video
N	Number of tiles or discrete viewing directions
$x_{n,l}$	Binary variable indicating that the client will prefetch tile n of the chunk at quality level l
$q_{n,l}$	Playback encoding of tile n of the chunk with quality level l
$b_{n,l} = b(q_{n,l})$	Size of tile n of the chunk with quality level l
$u_{n,l} = u(q_{n,l})$	Playback utility of playing tile n (direction n) of the chunk with quality level l
Δ	Playback duration of the chunk
D	Download rate
T	Average maintained buffer size in seconds
$E[u T]$	Expected playback utility, conditioned on T
$p_n(T)$	Probability looking in direction n , T time later
β	Parameter used to weight factors ($0 \leq \beta \leq 1$)

out the following optimization recursion:

$$DP(l_0, l, n, C) = \begin{cases} (1 - \beta)p_0 u(q_{0,l_0}) - \beta \frac{p_0 + p_1}{2} |u(q_{0,l_0}) - u(q_{1,l})|, & \text{if } n = 0, b_{0,l_0} \leq C \\ \max_{\{l' | b_{n,l'} + b_{0,l_0} \leq C\}} \left[(1 - \beta)p_n u(q_{n,l'}) \right. \\ \quad \left. - \beta \frac{p_n + p_{n+1}}{2} |u(q_{n,l}) - u(q_{n+1,l'})| \right. \\ \quad \left. + DP(l_0, l', n - 1, C - b_{n,l'}) \right], & \text{if } 1 \leq n \leq N - 1 \end{cases} \quad (9)$$

with the boundary cases that $DP(l_0, l, n, C) = -\infty$ whenever $b_{n,l} + b_{0,l_0} > C$. Given this recursion, the optimal solution can be calculated by considering all choices for direction 0; i.e., $\max_{0 \leq l \leq L} DP(l, l, N - 1, D\Delta)$. Algorithm 1 summarizes the calculations, from which the optimal solution is obtained through parent pointers.

Runtime analysis: There are $\Theta(CNL^2)$ sub-problems. Each takes $\Theta(L)$ to calculate, resulting in a total run-time of $\Theta(CNL^3)$.

5.4 Example characterization

Using the above optimization formulation, we next characterize the optimized prefetch aggressiveness tradeoff. Throughout the experiments presented in this section we assume encoding rates proportional to those found in an example YouTube video (equal to: 144, 268, 625, 1124, 2217, 4198 kbps) and present results for different prefetch capacities $C = D\Delta$ (the number of bytes that can be downloaded during a timeslot), the four different video categories considered in the paper, and four different utility functions: (i) a linear model, (ii) a square-root model, (iii) a logarithmic model, and (iv) a large-screen model proposed by Vleeschauwer et al. [31]:

$$u(q) = b \cdot \frac{(q/\theta)^{1-a} - 1}{1 - a}, \quad (10)$$

where $a > 1$, $b > 0$ and $\theta > 0$ are screen dependent parameters, in our case set to $a = 2$, $b = 10$, $\theta = 0.2Mbps$. Finally, a negative utility $u_{n,0}$ is used. In the experiments, we vary the stall penalty $\frac{u_{n,0}}{u_{n,L}}$ between -0.1 (small) to -100 (large).

To allow easier comparison, all utilization values were normalized such that the maximum utility (when played at the highest available quality encoding) was always 1. Furthermore, each tile could be selected in one of the discrete sizes: 144, 268, 625, 1124, 2217, 4198 “units” and the capacity C was measured in the

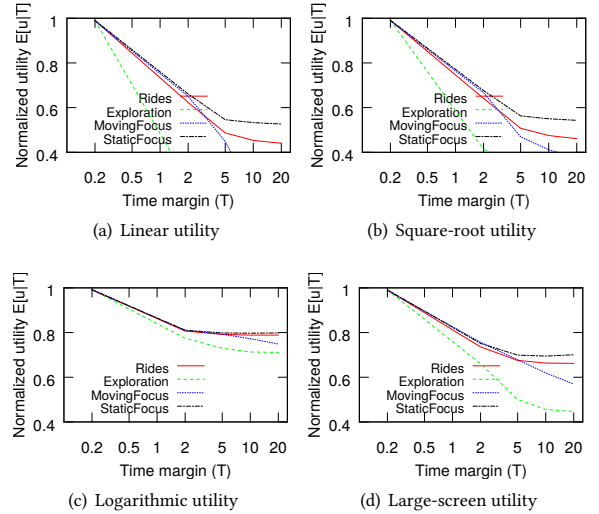


Figure 9: Example tradeoffs for different 360° video categories. ($C = 2500$ and $\frac{u_{n,0}}{u_{n,L}} = -1$ in all sub-arxiv-figs.)

same units. (These units allow us to avoid having to pick a chunk playback duration Δ .)

Figure 9 compares the tradeoff curves for the different video categories, with each sub-figure using a different utility function but the same prefetch capacity $C = 2500$, stall penalty $\frac{u_{n,0}}{u_{n,L}} = -1$, and $\beta = 0.001$. We note that in all cases the static focus and exploration categories provide the two extremes and the other two categories fall in between. Interestingly, all the static focus and rides curves flatten out after 5 seconds. This suggests that these categories can use prefetching to build larger buffers at little expense in expected utility. In contrast, moving focus and especially exploration typically have a more gradual tradeoff curve. For these categories, there are noticeable benefits to the expected utility (assuming stalls do not occur) when using more short-term prefetching; e.g., using $T = 5$ compared to $T = 20$, for example. However, since smaller buffers come at high risks, we note that these categories may benefit from more incremental prefetching algorithms in which each tile is gradually prefetched using layered encoding. In the next section we describe and discuss one such candidate solution.

Comparing the sub-arxiv-figs themselves, we note a general ordering between the utility functions. This is more clearly illustrated

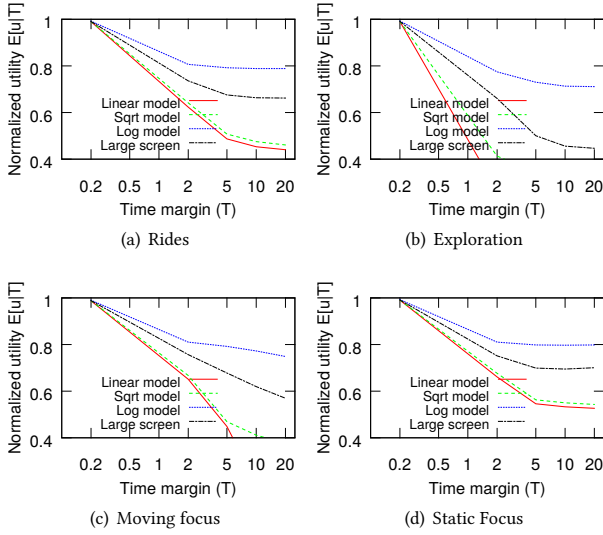


Figure 10: Example tradeoffs for different utility functions. ($C = 2500$, $\frac{u_{n,0}}{u_{n,L}} = -1$, $\beta = 0.001$.)

in Figure 10, where we have extracted the corresponding curves for each of the example categories. These results show that a user’s sensitivity to temporary quality degradations after sudden head movements (captured by the different utility functions) significantly impacts the importance of more accurate prediction, or as we will see next use of additional prefetch capacity. For example, the linear (pessimistic) assumption consistently results in the lowest utility, while the logarithmic (optimistic) assumption consistently results in the highest utility. For the remainder of this section, we focus on the large-screen model, which is motivated by existing work [31] and provides intermediate results.

To study the impact of various system parameters and conditions, we next show example results for each of the four categories, but note that static focus and exploration typically represent the two extreme categories, with the results for the other two categories typically falling in between, the results for rides being more similar to those of static focus and the results for moving focus being more similar to the exploration results. Throughout this analysis we use the large-screen utility function, consider one parameter at a time, and use the following default values: penalty factor $\frac{u_{n,0}}{u_{n,L}} = -1$, $\beta = 0.001$, and capacity $C = 2500$.

Diminishing prefetch capacity returns: Figure 11 illustrates the impact of the capacity C . We observe diminishing returns from doubling the capacity (from 1,250 all the way up to 20,000) and note that even a capacity of 5000 is able to achieve a utility of 0.837 and 0.737 even with $T = 20$ seconds. For static focus this is achieved by selecting rates somewhat more aggressive rates towards the front (with tile qualities: 1×2217 , 4×625 , 1×268), than for the exploration category (2×1124 , 4×625).

Limited impact of stall penalty: Figure 12 shows example tradeoffs for different stall penalty factors $\frac{u_{n,0}}{u_{n,L}}$, ranging from small (-0.1) to large (-100). We note that there only are very small differences observed here. In fact, for capacities $C = 5000$ and larger, the

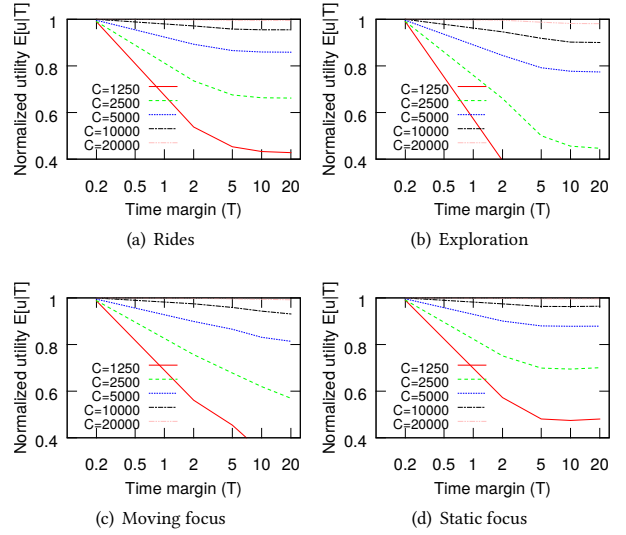


Figure 11: Example tradeoffs for different capacities. (Large-screen utility function with $\frac{u_{n,0}}{u_{n,L}} = -1$ and $\beta = 0.001$.)

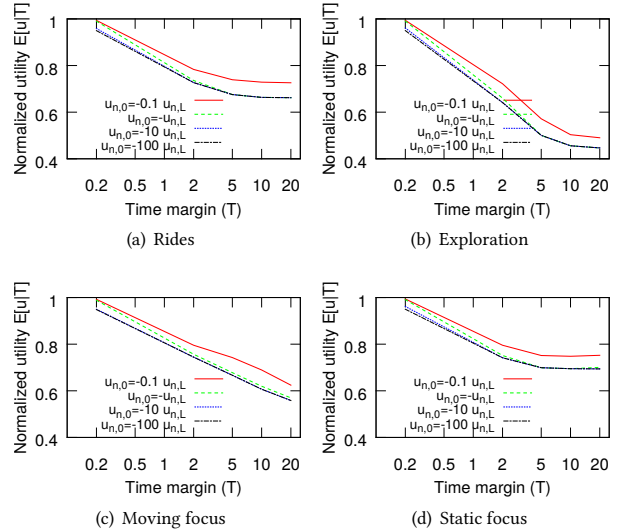


Figure 12: Example tradeoffs for different penalties $\frac{u_{n,0}}{u_{n,L}}$. (Large-screen utility function with $C = 2500$ and $\beta = 0.001$.)

results are independent of the stall penalty, since the optimal solutions with these capacities always involved obtaining at least the lowest encoding rate for each tile. This highlights the importance of always protecting against stalls.

Impact of weight given to quality differences between neighboring tiles: While we expect that the most realistic β typically would be small, we have experimented with different β values. In general, a larger (negative) β factor does not impact the quality choices substantially, but does shift the weighted utility curves downwards. This is illustrated by comparing Figure 13 (with $\beta = 0.25$) and Figure 11 (with $\beta = 0.001$). As expected, we have found that there are somewhat more evenly distributed quality selections with $\beta = 0.25$. For example, the right-most points for the $C = 5000$

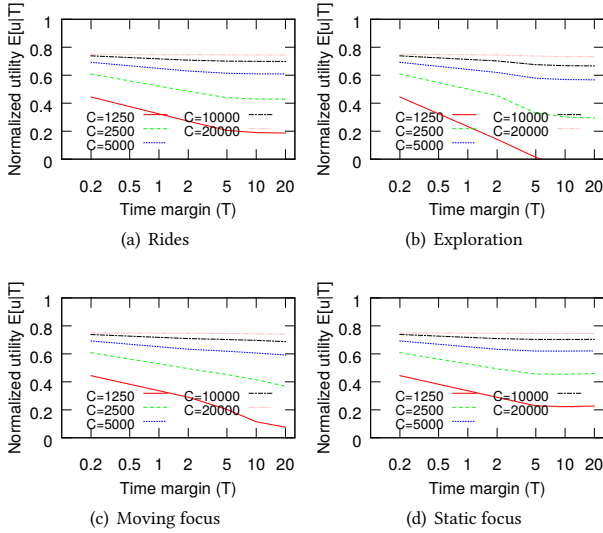


Figure 13: Capacity tradeoffs with large $\beta = 0.25$. (Large-screen utility function with $\frac{u_{n,0}}{u_{n,L}} = -1$.)

curves for static focus (which we discussed above) now use $(3 \times 1124, 2 \times 625, 1 \times 268)$, compared to $(1 \times 2217, 4 \times 625, 1 \times 268)$ with $\beta = 0.001$. For exploration, the two optimal solutions are identical. For similar reasons, we see somewhat flatter tradeoff curves with static focus when β increases, whereas they remain similar for the exploration category. Again, remember that the absolute utilities in the two different plots should not be compared against each other, only the relative shapes, since they represent substantially different utility models. Yet, the high β results show that the insights obtained for smaller β also hold for larger β .

Impact of number of tiles: The qualitative tradeoff results and general differences between the different categories presented here also hold when using other number of tiles. This is exemplified in Figure 14, which shows example results when using $N = 12$ tiles instead of $N = 6$ tiles. In particular, the three rows in Figure 14 shows the $N = 12$ results corresponding to the $N = 6$ results in Figures 9, 10 and 11, respectively. To allow a fair comparison, using our normalized per-tile units, we use double the per-chunk capacity C .

6 DISCUSSION OF FURTHER DESIGN OPTIMIZATIONS

When considering the optimal solutions, at both short and long time scales T , it is typically optimal to download some minimum quality in each viewing direction so as to protect against stalls (or missing tiles). Motivated by this observation we argue that prefetching can be split over multiple time scales.

Framework to split prefetching across time scales: In the following we describe a simple framework that allows us to simultaneously perform both (i) long-term prefetching so to protect against bandwidth variations and other unforeseen service outages, for example, and (ii) fine grained optimized prefetching based on the current viewing direction, as best done closer to the playback deadline. In its simplest form, a client separates the prefetching

process into two (or more) modules that operate in parallel. The first module is responsible for prefetching an initial base layer (e.g., based on SVC technology) for all viewing directions and can use a large buffer (e.g., 20-120 seconds). The latter prefetching module(s) then prefetch additional enhancement layers for each tile based on more up-to-date view-direction predictions.

For simplicity, let us assume that we use two modules. For this case, the optimization problem that must be solved by the second module, can easily be derived using a modified version of the optimization problem (and solution) described and evaluated in Section 5. In particular, assuming that the client has tile quality l' in direction n , we can simply use $b_{n,l} = 0$ for all $l \leq l'$, capturing that we already have tile quality l' for this direction. For the other tile qualities, the size will depend on whether some form of layered coding is implemented or not. For example, in the ideal case, assuming “perfect” SVC without any overhead, we would have $b_{n,l} \approx \Delta(q_{n,l} - q_{n,l'})$. At the other extreme, assuming that tiles would need to be completely re-downloaded at a higher quality level, we would have $b_{n,l} \approx \Delta q_{n,l}$. Naturally, different implementations will fall somewhere in between these two extremes.

Figure 15 shows the example layers that a client has prefetched in each step, when using SVC together with three prefetching modules. Here, the first module (A) made its decision at time T_A (e.g., 15 seconds before the playback deadline) based on viewing direction $(0, 1)$, the second module (B) based on a direction $(\frac{\sqrt{3}}{2}, \frac{1}{2})$ and the final module (C) based on viewing direction $(1, 0)$. In each step, the previously prefetched tile qualities are leveraged so to best use the available prefetching capacity of that module, each module solving the above optimization problem.

We next use our measurements to study additional biases that can be used to further optimize the final quality selections.

Short-term biases based on velocity: Not surprisingly, over short time scales, there is strong correlation between the direction of head movement and the future viewing direction. Figure 16 shows the change in yaw-angle after 200 ms for all videos, when the user’s current velocity was higher than $\pm 5^\circ$ per second ($\pm 5^\circ/s$, for short). Here, a positive (negative) velocity means that a user is turning to the left (right).

Even with a small velocity threshold of $\pm 5^\circ/s$ (with 55% of all readings having a larger directional velocity), in 97% of these cases the eventual view angle is strictly in the direction suggested by the head movement direction 200 ms earlier. The results are even stronger if using a small (additional) safety angle. For example, in 99.9% of the cases, the direction is no further in the opposite direction than 9° and 7° , respectively. This is due to head movements being relatively smooth and shows that there is potential for shrinking the range of angles that the point-of-view is likely to be rotated to next. For example, referring back to Figure 7 we note that the user’s view is expected to change no more than $\pm 46^\circ$ 99% of the time. However, as per the above examples, in more than half of the cases this range can be cut by 40.2% and 42.4%, respectively, if also taking into account the current velocity. This shows that for the final enhancements (prefetched over shorter time scales), it is possible to further improve prediction accuracy.

We have observed clear biases for time scales up to 2 seconds. Figure 17 shows the prediction error rates when predicting left

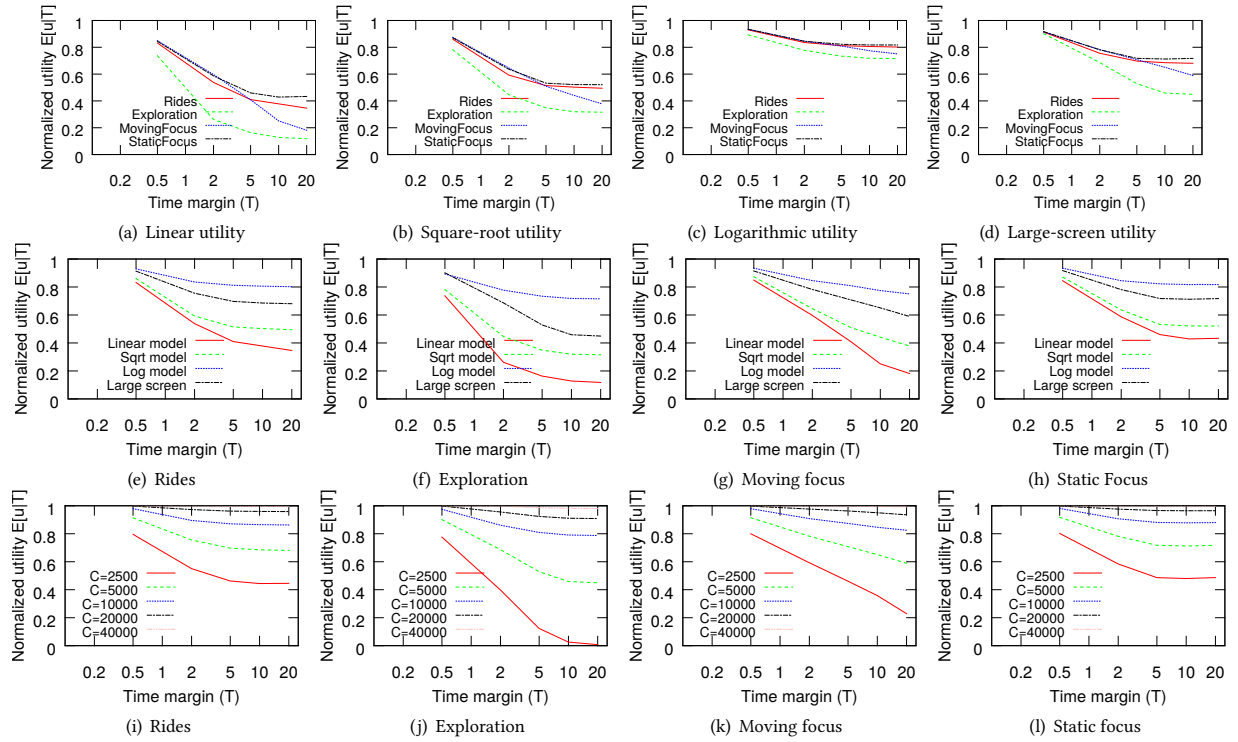


Figure 14: Example tradeoffs with twice as many tiles $N = 12$ as in Figures 9, 10 and 11. (Default settings: $C = 5000$, $\frac{u_{n,0}}{u_{n,L}} = -1$, $\beta = 0.001$ using large-screen model.)

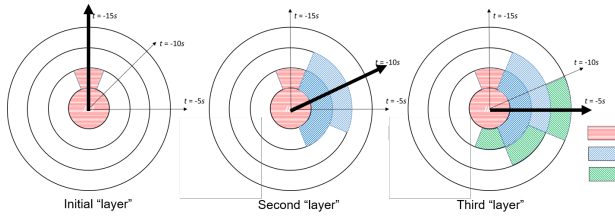


Figure 15: Example of personalized “layers” based on viewing direction and downloaded tiles.

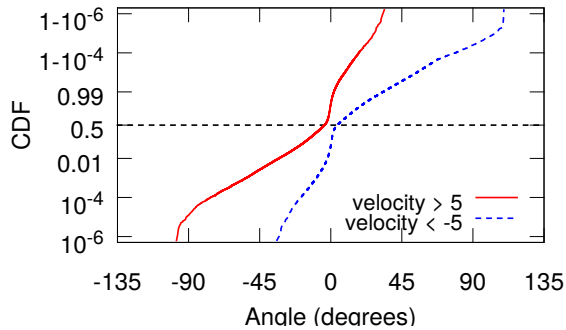


Figure 16: Change in angle over the next $T=200\text{ms}$ when velocity is greater than $\pm 5^\circ/\text{s}$.

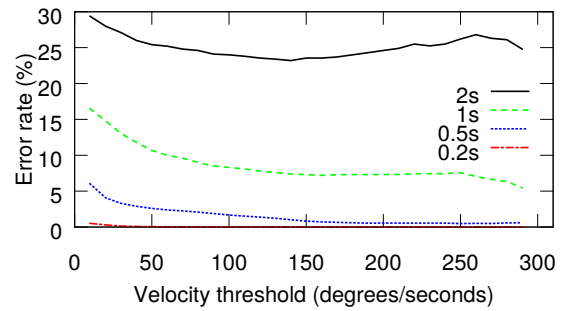


Figure 17: Prediction error rate when using current velocity to predict directional change; different prediction intervals.

or right movement based on the current velocity direction over different time intervals T : 0.2s, 0.5s, 1s and 2s. Here, the error rate is measured as the fraction of cases that the user’s viewpoint did not end up in the same relative direction as suggested by its velocity T seconds earlier. For these results we varied the velocity threshold. As expected, the accuracy typically improves with larger thresholds. (The bump for the 2 second curve can partially be explained by instances where users turn more than 180 degrees.) While the tighter thresholds result in smaller error rates, there are fewer instances that meet these criteria. Given the relatively flat curves, a relatively small threshold may therefore often be beneficial, using a small extra safety margin (as in the example in Figure 17), of course, so to protect against fast back-and-forth directional changes.

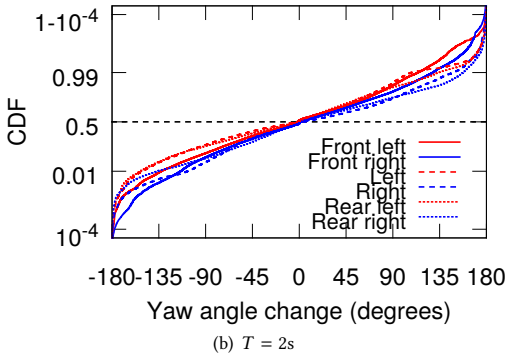
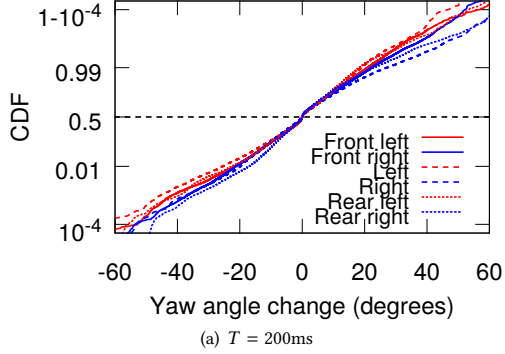


Figure 18: Change in yaw angle, conditioned on the viewers' location in the sphere. Exploration category.

Biases towards the origin: Perhaps the most challenging category to predict is the exploration category. Interestingly, even for this category, viewers are more likely to look in the same direction as when playback began, also later during the playback (e.g., in Figure 3). This may suggest that a user that currently looking to the right of the original starting direction may be more likely to perform large rotations to the left, and vice versa. To glean some insight whether this allows us to improve prediction for the exploration videos, Figure 18 plots the changes in yaw angle when the viewpoint was initially located in a certain part of the sphere. Here, the sphere was divided into 60° parts, starting from the 0° line. Results are shown for the change over both 200ms and 2s.

The bias is perhaps easiest observed by comparing the relative ordering of the lines. For example, the Left lines (currently looking to the left) tend to result larger negative (rightward) head movements than the Right lines and vice versa. When discussing these results, it should, however, be noted that for the exploration category, left and right rotations are as likely to occur no matter where the user is looking. For example, 50% of all rotation are less than zero and the 50% are larger than zero for all lines, limiting the improvements that the above biases may provide.

Reduced exploration over time: Referring back to our discussion of Figure 5, we have found that users tend to explore more at the beginning of a video and that the head movements typically reduce over time. This is also illustrated in Figure 19, where we show the viewing angle of three example viewers watching the Christmas

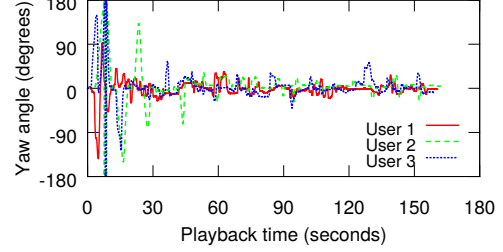


Figure 19: Viewing direction of three example users watching the Christmas scene (from the Static focus category).

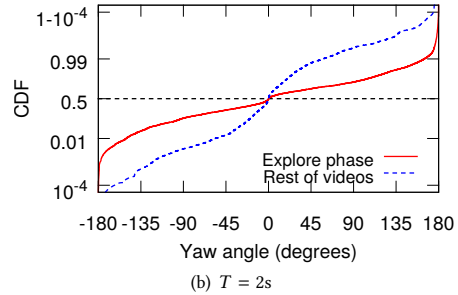
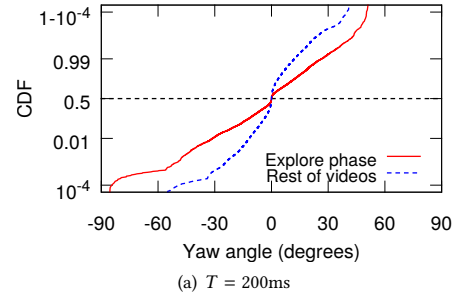


Figure 20: Change in view angle conditioned on users being in initial 20 second exploration phase or later in the videos.

scene video (from the static focus category). During the first 20 seconds, there is a lot of head movements as each user explores almost every yaw angle. Once the users have learned where the focus should be, the viewing angle stays relatively stable, centered roughly between $\pm 30^\circ$. This behavior has been observed for many users for most of the static focus and rides videos.

This shows that it may be possible to be more restrictive in the prefetched viewing angles. To quantify these effects, consider Figure 20. Here, we show the CDFs (on dual-log scales) for the change in yaw angle during the exploration phase (first 20 seconds) versus the rest of the video. Results are shown across all users, when the view change is measured over both 200 ms and 2s. For the case when measuring changes over 200ms, 99% of the changes after the exploration phase are smaller than $\pm 15^\circ$ compared to $\pm 39^\circ$ for the exploration phase. The corresponding 99.9% ranges are $\pm 24^\circ$ and $\pm 49^\circ$. When measuring changes over 2s, the differences are smaller but still noticeable. For example, the 99% ranges reduce from $\pm 164^\circ$ to $\pm 77^\circ$ and the 99.9% ranges from $\pm 178^\circ$ to $\pm 122^\circ$.

Although prediction schemes could benefit from adjusting the parameters used for predictions over the duration of a video, the video content is an important factor. Analysis of individual videos may be required to learn how each video is best divided so to optimize the prefetching. In this paper, we primarily compare categories of videos (rather than individual videos) across different time scales. Fine grained optimizations such as the ones discussed in this paragraph (or when discussing moving focus optimizations that take into account prior viewers of that video) remain future work.

7 RELATED WORK

While it is common that the whole 360° view is streamed to a client in a single chunk with a consistent encoding rate across the frame, different projection and quality adaptive download techniques are being used by some of the most popular 360° HMDs [34]. We are also not the first to consider the possibility of adaptively downloading different qualities for different viewing directions [4, 13] or to characterize 360° viewer behavior [8, 16].

Some of the most important challenges in this area include user head movement tracking/prediction [4, 24] and bandwidth management [13, 21]. Bao et al. [4] propose a motion-prediction-based transmission scheme that reduces bandwidth consumption during streaming of 360° videos. The prediction scheme is based on viewing behavior data collected similarly to this paper, but with substantially shorter user sessions and without categorizing videos. Yet, their findings suggest that view-dependent 360° transmission schemes with motion prediction can reduce bandwidth consumption by 45% at the cost of only very small performance degradation.

Others have shown significant storage and bandwidth savings by converting the equirectangular representation typically used to store 360° videos to a cube map layout [22], performed QoE-based measurement studies [26], and studied the impact that projection techniques, quantization parameters, and tile patterns may have on the playback experience and resource requirements [11]. The usage of tiles allows for independent encoding of different regions of a frame. This helps the decoder, both in terms of potential decoding parallelism and in selective reconstruction of parts of the frame.

Hosseini and Swaminathan [13] propose an adaptive tile-based streaming approach for bandwidth-efficient streaming of 360° videos. The system spatially divides a 360° video's equirectangular representation into several tiles, utilizes MPEG-DASH Spatial Representation Description (SRD) [20] to describe the spatial relationship between the tiles, and then prioritizes the tiles based on the user's field of view. Again, large bandwidth savings (72%) are demonstrated with only small quality degradation. Hamza and Hefeeda [10] illustrate how a client can be implemented to make use of the SRD to find the available resolution layers, select the most appropriate ones and enabling a seamless switch when panning between spatial regions of a video.

Rather than using tiles, Kuzyakov and Pio [23] present a view-dependent streaming technique for 360° video that efficiently utilizes bandwidth by transforming the original video into 30 smaller sized versions, where each version has a specific area in high quality, gradually decreasing the quality away from this area.

Several prior works have demonstrated interactive tiled streaming of high-resolution videos [9, 25, 30]. This includes delivery of

ultra-high resolution videos based on a user's region-of-interest [17, 18]. Others have used tile-based spatial segmentation to support pan/tilt/zoom interactions during live streaming [30], for interactive 4k video delivery during the 2014 Commonwealth games [25], and for a coaching/training application [9].

Within the context of HAS, the tradeoff between accurate prefetching based on expected user behavior and eventual quality of experience has also been analyzed for other forms of interactive media, including multi-view video [6, 28], branched video [14], and free-viewpoint video [12, 32]. For all these types of video the simplest method is to download the entire video (or set of views) but significant download savings are possible by carefully and adaptively prefetching different areas of the video at different encoding rates.

In contrast to the above 360° works, we consider longer sessions in which the users watch different categories of videos, we characterize the viewing behavior within and across these video categories, and we use an optimization framework to both qualitatively and quantitatively characterize the general prefetch aggressiveness tradeoff described and analyzed in this paper.

8 CONCLUSIONS

This paper presents a data-driven characterization of the prefetching aggressiveness tradeoff associated with how far ahead in time from the current play point prefetching should be done. In particular, we collect head movement data for 32 users as they watch a set of 30 videos a total of 439 times. Using this data, we then characterize user behavior for four different categories of 360° videos (i.e., static focus, moving focus, rides, and exploration) and provide both qualitative and quantitative insights regarding how best to address the prefetching aggressiveness tradeoff.

In general, we have observed significant differences among the video categories with respect to the predictability of the viewpoint at different time scales, and hence on the granularity with which view-based prefetching can be done. As expected, the highest predictability is achieved over short time ranges. To explore the prefetching aggressiveness tradeoff more precisely, we presented an optimization problem that we solved using dynamic programming, allowing us to study the optimized tradeoff curves. Based on the insights provided by the optimization model, we then discuss other system optimizations and measurement-based biases that can be used to further improve the user's quality of experience.

Acknowledgements: The authors are thankful to the participants of the study and to our shepherd Simon Gunkel and the anonymous reviewers for their feedback. This work was funded in part by the Swedish Research Council (VR) and the Natural Sciences and Engineering Research Council (NSERC) of Canada.

REFERENCES

- [1] M. Abrash. 2014. What VR Could, Should, and almost certainly Will be within two years. (2014). <http://media.steampowered.com/apps/abrashblog/Abrash%20Dev%20Days%202014.pdf>
- [2] R. S. Allison, L. R. Harris, M. Jenkin, U. Jasiobedzka, and J. E. Zacher. 2001. Tolerance of temporal delay in virtual environments. In *Proc. IEEE Virtual Reality*.
- [3] M. Almqvist, V. Almqvist, V. Krishnamoorthi, N. Carlsson, and D. Eager. 2018. The Prefetch Aggressiveness Tradeoff in 360 Video Streaming. In *Proc. ACM MMSys*.
- [4] Y. Bao, H. Wu, T. Zhang, A. Ramli, and X. Liu. 2016. Shooting a moving target: Motion-prediction-based transmission for 360-degree videos. In *Proc. IEEE Big Data*.

- [5] L. M. Batteau, A. Liu, J. A. Maintz, Y. Bhasin, and M. W. Bowyer. 2004. A study on the perception of haptics in surgical simulation. *Medical Simulation, Springer* (2004), 185–192.
- [6] N. Carlsson, D. Eager, V. Krishnamoorthi, and T. Polishchuk. 2017. Optimized Adaptive Streaming of Multi-video Stream Bundles. *IEEE Transactions on Multimedia* 19 (July 2017), 1637–1653.
- [7] X. Corbillon, G. Simon, A. Devlic, and J. Chakareski. 2017. Viewport-adaptive navigable 360-degree video delivery. In *Proc. IEEE ICC*.
- [8] X. Corbillon, F. D. Simone, and G. Simon. 2017. 360Degree Video Head Movement Dataset. In *Proc. ACM MMSys*.
- [9] L. D’Acunto, J. Redi, and O. Niamut. 2015. iCaCoT - Interactive Camera-Based Coaching and Training. In *Proc. Workshop on Interactive Content Consumption*.
- [10] L. D’Acunto, J. van den Berg, E. Thomas, and O. Niamut. 2016. Using MPEG DASH SRD for zoomable and navigable video. In *Proc. ACM MMSys*.
- [11] M. Graf, C. Timmerer, and C. Mueller. 2017. Towards Bandwidth Efficient Adaptive Streaming of Omnidirectional Video over HTTP: Design, Implementation, and Evaluation. In *Proc. ACM MMSys*.
- [12] A. Hamza and M. Hefeeda. 2016. Adaptive Streaming of Interactive Free Viewpoint Videos to Heterogeneous Clients. In *Proc. ACM MMSys*.
- [13] M. Hosseini and V. Swaminathan. 2016. Adaptive 360 VR video streaming: Divide and conquer. In *Proc. IEEE ISM*.
- [14] V. Krishnamoorthi, N. Carlsson, D. Eager, A. Mahanti, and N. Shahmehri. 2014. Quality-adaptive prefetching for interactive branched video using HTTP-based adaptive Streaming. In *Proc. ACM Multimedia*.
- [15] S. M. LaValle, A. Yershova, M. Katsev, and M. Antonov. 2014. Head tracking for the Oculus Rift. In *Proc. IEEE ICRA*.
- [16] W. Lo, C. Fan, J. Lee, C. Huang, K. Chen, and C. Hsu. 2017. 360 Video Viewing Dataset in Head-Mounted Virtual Reality. In *Proc. ACM MMSys*.
- [17] A. Mavlankar, P. Baccichet, D. Varodayan, and B. Girod. 2007. Optimal Slice Size for Streaming Regions of High Resolution Video With Virtual Pan/Tilt/Zoom Functionality. In *Proc. European Signal Processing Conference*.
- [18] A. Mavlankar, P. Agrawal, D. Pang, S. Halawa, N. Cheung, and B. Girod. 2010. An Interactive Region-of-Interest Video Streaming System for Online Lecture Viewing. In *Proc. Packet Video Workshop*.
- [19] S. K. Nayar. 1997. Catadioptric omnidirectional camera. In *Proc. IEEE CVPR*.
- [20] O. Niamut, E. Thomas, L. D’Acunto, C. Concolato, F. Denoual, and S. Y. Lim. 2016. MPEG DASH SRD: spatial relationship description. In *Proc. ACM MMSys*.
- [21] D. Ochi, Y. Kunita, K. Fujii, A. Kojima, S. Iwaki, and J. Hirose. 2014. HMD viewing spherical video streaming system. In *Proc. ACM Multimedia*.
- [22] D. Pio and E. Kuzyakov. 2015. Under the hood: Building 360 video. (Oct. 2015). <https://code.facebook.com/posts/1638767863078802/under-the-hood-building-360-video/>
- [23] D. Pio and E. Kuzyakov. 2016. Next-generation video encoding techniques for 360 video and VR. (Jan. 2016). <https://code.facebook.com/posts/1126354007399553/next-generation-video-encoding-techniques-for-360-video-and-vr/>
- [24] F. Qian, L. Ji, B. Han, and V. Gopalakrishnan. 2016. Optimizing 360 video delivery over cellular networks. In *Proc. All Things Cellular Workshop*.
- [25] J. Redi, L. D’Acunto, and O. Niamut. 2015. Interactive UHD TV at the Commonwealth Games: An Explorative Evaluation. In *Proc. ACM TVX*.
- [26] R. Schatz, A. Sackl, C. Timmerer, and B. Gardlo. 2017. Towards subjective quality of experience assessment for omnidirectional video streaming. In *Proc. QoMEX*.
- [27] M. Seufert, S. Egger, M. Slanina, T. Zinner, T. Hoßfeld, and P. Tran-Gia. 2015. A Survey on Quality of Experience of HTTP Adaptive Streaming. *IEEE Communications Surveys Tutorials* 17, 1 (2015), 469–492.
- [28] T. Su, A. Sobhani, A. Yassine, S. Shirmohammadi, and A. Javadtalab. 2016. A DASH-based HEVC multi-view video streaming system. *Journal of Real-Time Image Processing* 12, 2 (2016), 329–342.
- [29] Z. Tan, Y. Li, Q. Li, Z. Zhang, Z. Li, and S. Lu. 2018. Enabling Mobile VR in LTE Networks: How Close Are We?. In *Proc. ACM SIGMETRICS*.
- [30] R. van Brandenburg, O. Niamut, M. Prins, and H. Stokking. 2011. Spatial segmentation for immersive media delivery. In *Proc. ICIN*.
- [31] D. D. Vleeschauwer, H. Viswanathan, A. Beck, S. Benno, G. Li, and R. Miller. 2013. Optimization of HTTP adaptive streaming over mobile cellular networks. In *Proc. IEEE INFOCOM*.
- [32] X. Xiu, G. Cheung, and J. Liang. 2012. Delay-cognizant interactive streaming of multiview video with free viewpoint synthesis. *IEEE Trans. on Multimedia* 14, 4 (2012), 1109–1126.
- [33] X. Yin, A. Jindal, V. Sekar, and B. Sinopoli. 2015. A Control-Theoretic Approach for Dynamic Adaptive Video Streaming over HTTP. In *Proc. ACM SIGCOMM*.
- [34] C. Zhou, Z. Li, and Y. Liu. 2017. A Measurement Study of Oculus 360 Degree Video Streaming. In *Proc. ACM MMSys*.